instruments

MDPI

Article

A 3D Printed Air-Tight Cell Adaptable for Far-Infrared Reflectance, Optical Photothermal Infrared Spectroscopy, and Raman Spectroscopy Measurements

Annalisa Paolone [1,2,*], Arcangelo Celeste [3], Maria Di Pea [2,3], Sergio Brutti [2,3], Ferenc Borondics [4] and Francesco Capitani [4]

[1] Consiglio Nazionale delle Ricerche, Istituto dei Sistemi Complessi, UOS Sapienza, Piazzale Aldo Moro 5, 00185 Rome, Italy
[2] GISEL-Centro di Riferimento Nazionale per I Sistemi di Accumulo Elettrochimico di Energia, INSTM via G. Giusti 9, 50121 Firenze, Italy; mariadipea@gmail.com (M.D.P.)
[3] Department of Chemistry, Sapienza University of Rome, Piazzale Aldo Moro 5, 00185 Rome, Italy; arcangelo.celeste@uniroma1.it
[4] Synchrotron SOLEIL, L'Orme des Merisiers, Départementale 128, 91190 Saint-Aubin, France; ferenc.borondics@synchrotron-soleil.fr (F.B.); francesco.capitani@synchrotron-soleil.fr (F.C.)
* Correspondence: annalisa.paolone@roma1.infn.it

Abstract: Material characterization and investigation are the basis for improving the performance of electrochemical devices. However, many compounds with electrochemical applications are sensitive to atmospheric gases and moisture; therefore, even their characterization should be performed in a controlled atmosphere. In some cases, it is impossible to execute such investigations in a glove box, and, therefore, in the present work, an air-tight 3D printed cell was developed that preserves samples in a controlled atmosphere while allowing spectroscopic measurements in reflectance geometry. Equipped with a cheap 1 mm thick CaF_2 optical window or a more expensive 0.5 mm thick ZnS window, the cell was used for both optical photothermal infrared and Raman spectroscopy measures; imaging of the samples was also possible. The far-infrared range reflectance measurements were performed with a cell equipped with a diamond window.

Keywords: 3D printing; optical photothermal infrared spectroscopy; Raman spectroscopy; infrared spectroscopy; air-tight cell

Citation: Paolone, A.; Celeste, A.; Di Pea, M.; Brutti, S.; Borondics, F.; Capitani, F. A 3D Printed Air-Tight Cell Adaptable for Far-Infrared Reflectance, Optical Photothermal Infrared Spectroscopy, and Raman Spectroscopy Measurements. *Instruments* **2024**, *8*, 54. https://doi.org/10.3390/instruments8040054

Academic Editor: Antonio Ereditato

Received: 31 October 2024
Revised: 7 December 2024
Accepted: 10 December 2024
Published: 16 December 2024

1. Introduction

The last years have witnessed an increased interest in energy storage devices due to the request for more sustainable and eco-friendly systems [1]. Among the various systems for energy storage, electrochemical devices have gained a preponderant role, especially for their applications in portable devices and for vehicle traction [2]. Lithium-ion and post-lithium-ion batteries are certainly the best-known electrochemical devices [3].

The development of new materials, their investigation, and characterization are the main ingredients to improve the performance of batteries. However, this research also poses some challenges, such as the high reactivity of electrodes and electrolytes with air and moisture. For this reason, a major part of the research on battery materials is performed in glove boxes, although several experimental setups are not compatible with such a confined environment. In this framework, it is useful to develop cells where materials under investigation can be preserved from external contamination while allowing access to the samples for the experimental probe of choice. The purpose of this study was to develop a cell that allowed measurements using optical photothermal infrared spectroscopy and Raman spectroscopy of as-prepared or post-mortem electrodes of batteries. We have previously reported the applications of such spectroscopic techniques to investigate the

Solid–Electrolyte interphase developed on Si nanowires cycled in electrolytes based on organic carbonates [4].

The concept of using a cell equipped with an optical window is not new. Cells have been widely used when samples are cooled down to below room temperature. However, these kinds of cells have been typically built from metals in specialized mechanical workshops. In the last few years, the development of widespread and easy-to-use 3D printers able to create objects from fused polymers has revolutionized this field [5]. Indeed, many applications of 3D printing to spectroscopy, imaging, and electrochemistry have been proposed in the last five years: a microfluidic circuit with vacuum sealing [6], a cell for fluorescence imaging [7], low-cost microscopes [8,9] and several applications in the field of electrochemistry, such as flow cells [10,11], cells for optical microscopy [12,13] or spectroscopic investigations [14–16] coupled to electrochemical measures.

Among the experimental methods useful to investigate materials for batteries, we focused our attention on optical photothermal infrared spectroscopy (OPTIR), Raman spectroscopy, and far-infrared reflectance. All these techniques work in a specular reflectance geometry, even though they are based on different physical phenomena. For far-infrared reflectance measurements, a beam of infrared light in the wavenumber range of 100–700 cm^{-1} hits the sample almost at a normal incidence, and the light reflected by the sample at the same wavenumber is measured. On the other hand, the configuration used in the present study, and in most Raman microscopes, is based on a laser beam hitting the sample through an optical objective at normal incidence; the intensity of the light backscattered in the objective at wavelengths slightly different from that of the laser is recorded. Finally, optical photothermal infrared spectroscopy (OPTIR) is a relatively new technique that allows measuring the infrared absorption of samples through the photothermal effect. In detail, the sample is illuminated at normal incidence by a beam of mid-IR light generated by quantum cascade lasers (QCLs). When QCLs are tuned to wavelengths that excite molecular vibrations in the sample, absorption occurs. This generates a sample surface expansion and a change in refractive index (photothermal effects). A visible green laser measures this photothermal response via a modulation induced in the scattered light. The OPTIR technique can overcome the diffraction limit of traditional IR microscopy because the detecting radiation is in the visible range, and, therefore, it allows monitoring the variation of the spectrum of the sample on a sub-micron length scale. OPTIR is also useful as it is a non-contact technique, contrary to Attenuated Total Reflectance, which has been largely used to investigate electrodes for batteries.

Due to the different wavelengths of the light beams used in the three experimental techniques, different transmittance spectral ranges are required for the cell's optical window, depending on the application. For Raman spectroscopy, transmittance in the visible range is needed, and there is no requirement for infrared transmittance. For far-infrared reflectance measurements, the optical window should be transparent in the far-infrared range, and no requirements for the transmission in the visible range are set unless imaging of the sample could be interesting. The most stringent requirements are present for optical photothermal infrared spectroscopy measurements because, in this case, the optical window should be transparent both in the mid-infrared range to allow the excitation of the vibrational modes of the sample by the incident infrared laser light and in the visible range to allow the detection of the photothermal effects by the green laser. For this reason, we aimed to develop a simple 3D printed cell that could be adapted to various optical windows. In particular, cheap (EUR 7) CaF_2 windows can be used for Raman and OPTIR measurements, while more expensive (EUR 480) diamond windows are employed for the far-infrared reflectivity experiments.

2. Materials and Methods

Three-dimensional printed air-tight cells were made of the polylactic acid (PLA) polymer and printed on both an Ultimaker 3+ Connect and a Prusa i3 MK3 system at CNR in Rome. The

program to generate the cells was written using the OpenSCAD software [17]. Four cells were developed to adapt to different optical windows and experimental techniques:

(1) CaF_2 window, diameter 12 mm, thickness 1 mm, IR Grade, purchased from EKSMA Optics (Lithuania), cost about EUR 7 each for both OPTIR and Raman spectroscopy;
(2) ZnS window, diameter 12.7 mm, thickness 0.5 mm, purchased from Crystran, cost about EUR 35 each for both OPTIR and Raman spectroscopy;
(3) BaF_2 window, diameter 25.4 mm, thickness 2 mm, purchased from EKSMA Optics (Lithuania), cost about EUR 66 each for OPTIR spectroscopy;
(4) diamond window, diameter 10 mm, thickness 0.4 mm, purchased from Diamond Materials GmbH, cost about EUR 480 each for far-infrared reflectance measures.

All four types of optical windows are transparent in the visible range as they are colorless; however, they possess different transmittance properties in the mid-infrared range, as will be described in the following.

The tightness of the cells was assured by an O-ring in a static tight configuration with a cord diameter equal to 1.5 mm and with an external diameter of 10 mm for the diamond window and 12 mm for the CaF_2 and ZnS windows.

The shorter focal length of the objectives of the Raman, infrared, and OPTIR systems used to perform measurements was 9 mm, thus constraining the distance between the upper part of the cover and the plane where the sample seats. In the final version of the cells, this distance was about 5.5 mm, and the thickness of the sample could reach 1 mm without touching the inner face of the optical window. A drawing of the cell for the optical windows of CaF_2 is reported in Figure 1, and the STL files for the cells corresponding to points 1 and 2 of the previous list were deposited in the Zenodo repository (DOI: 10.5281/zenodo.13985862).

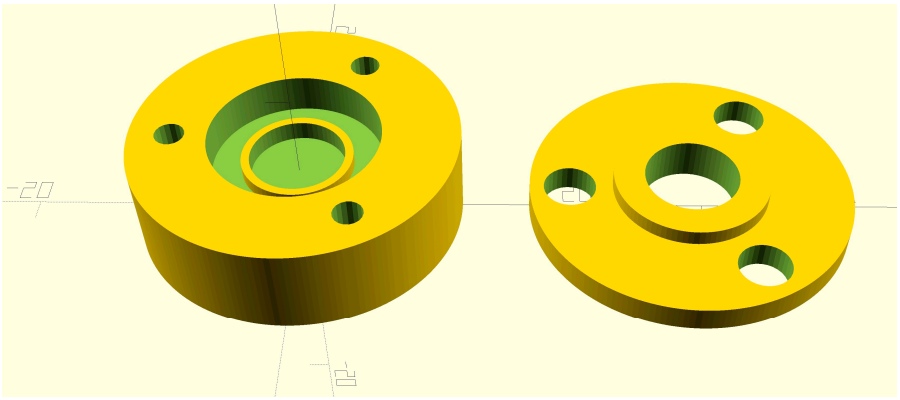

(**a**)

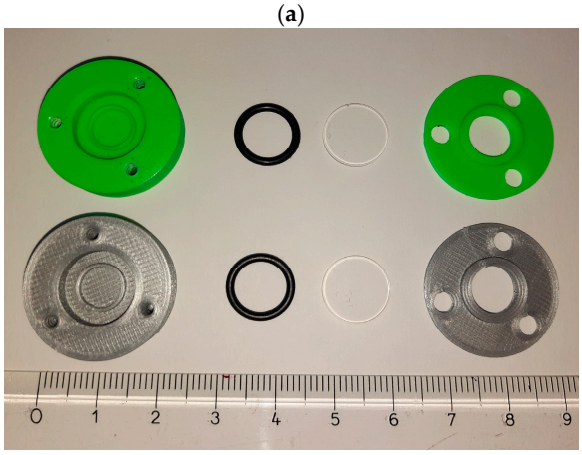

(**b**)

Figure 1. (**a**) Technical 3D drawing of the cell for the optical windows of CaF_2 (**left**) and the relative cover (**right**); (**b**) picture of the real opened cells obtained by two different 3D printers.

Some cells that allowed the containment of thicker samples were printed during the development phase to check for eventual leakages. To do so, some pieces of silica gel were put inside the cells; the cover was closed with the optical window in place, the cells were exposed to air for 15 days, and the color changes of the silica gel were checked, which is deep blue in its anhydrous state and becomes progressively pink upon hydration.

The OPTIR instrument used for the measurements was the mIRage system by Photothermal Spectroscopy Corp. at the SMIS beamline of Synchrotron Soleil, which covers the wavenumber range between 920 and 3100 cm^{-1}. Spectra reported in this paper were acquired through a 40× Schwarzschild objective (0.78 NA, 8 mm WD) in reflection mode, with a 2 cm^{-1} spectral resolution.

For Raman spectroscopy, we used the LabRAM Soleil Raman Microscope from the Chemistry Laboratories of Soleil developed by Horiba Scientific equipped with a long working distance Nikon objective 50×. Spectra were acquired between 50 and 3600 cm^{-1}, with a spectral resolution of about 2 cm^{-1}.

Far-infrared reflectance measurements were conducted at the SMIS beamline utilizing a Nicplan microscope/Thermo Fisher iS50 FTIR spectrometer equipped with a Si Bolometer, working between 100 and 700 cm^{-1}, with a spectral resolution of 4 cm^{-1}.

The infrared transmittance of the optical windows was measured at CNR in Rome employing an Agilent Cary 660 spectrometer with a DTGS detector and a KBr beamsplitter. The spectral resolution was fixed at 1 cm^{-1} in the wavenumber region between 420 and 6000 cm^{-1}. Raman spectra of the optical windows were collected by the LabRAM Soleil Raman Microscope of the Chemistry Laboratories of Soleil Synchrotron.

To verify the goodness of the spectra collected in the cells using various techniques, several samples were measured outside and inside the air-tight cells, and the acquired spectra were compared. $FeCO_3$ (purity $\geq$ 96%), $LiCoPO_4$ (purity $\geq$ 99%), and Li_2CO_3 (purity $\geq$ 99%) were purchased from Sigma Aldrich. Single-side optically polished Si wafers with a resistivity <0.002 Ohm cm were purchased from Siegert Wafer. Whatman® glass microfiber grade GF/A filter discs, with 1.6 µm pore size and 0.26 mm thickness, were purchased from Merck.

3. Results

3.1. Investigation of Air Tightness

First, to ascertain if the tightness of the cells was preserved over time, we printed cells with CaF_2 windows with a sample seat about 3 mm deep, where some grains of silica gel could be accommodated. The color of the grains was recorded over time in comparison with that of grains maintained in air. Figure 2 shows that silica gel in the air changes its color from blue to transparent/pink in a few hours; however, the cells could preserve the blue color even for 15 days.

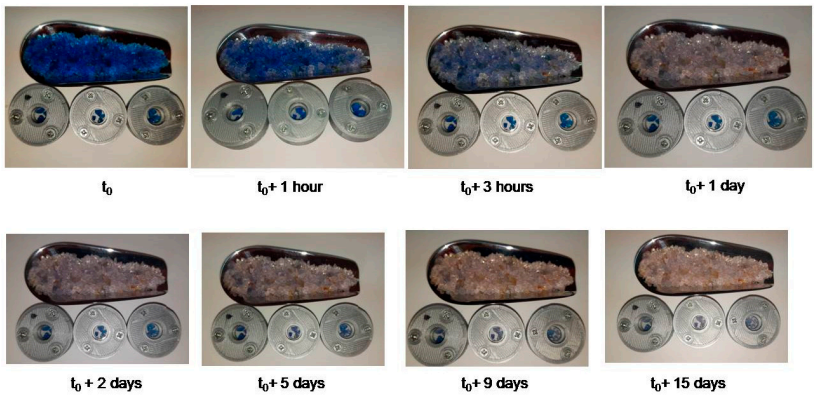

Figure 2. Pictures at different times of sealing test via silica gel color comparison between grains exposed to air and those maintained in the sealed cells for 15 days.

3.2. Infrared and Raman Spectra of the Optical Windows

The infrared transmittance and Raman scattering spectra of the bare optical windows used in this study were recorded. Figure 3 reports the IR transmittance measured between 400 and 6000 cm^{-1}, while Figure 4 displays the Raman spectra between 50 and 800 cm^{-1}. Diamond is transparent in the whole frequency range (see Figure 3) with a transmittance of about 0.7, even though some absorptions between 1700 and 4000 cm^{-1} are visible. They are due to the phonon modes and the impurities present in the material [18]. At lower frequencies, it is possible to observe a series of interference fringes due to the high parallelism of the window faces. It must be noted that these fringes perfectly compensate for the measured reflectance spectra.

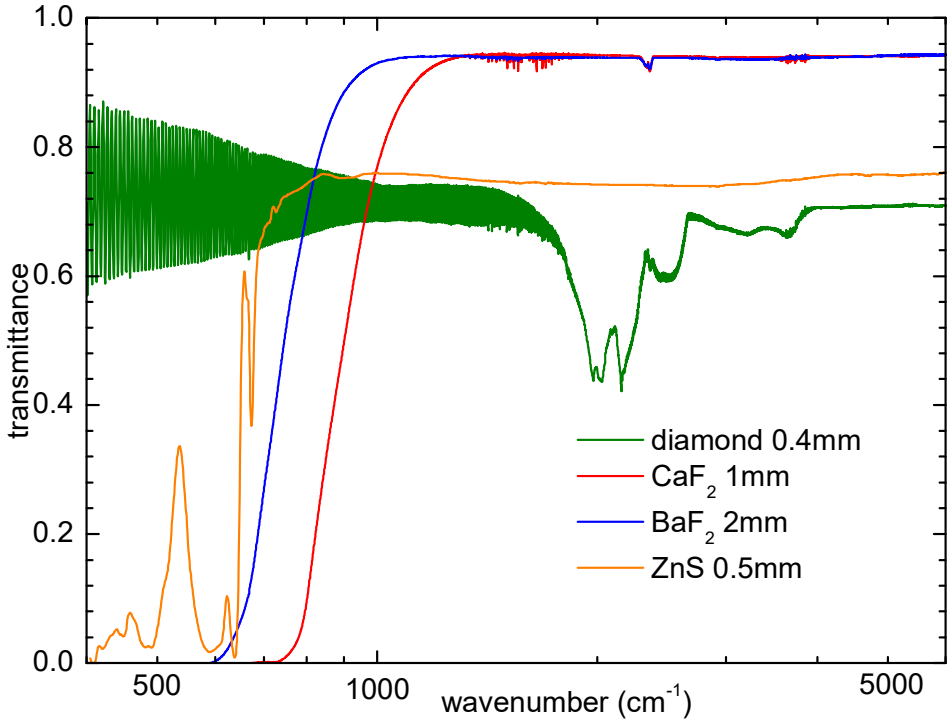

Figure 3. Infrared transmittance spectra of the CaF_2, diamond, BaF_2, and ZnS optical windows used in this study.

CaF_2 and BaF_2 had a 95% transmittance above 1300 and 1050 cm^{-1}, respectively. Their transmittance decreased to 50% at 900 and 745 cm^{-1}, respectively, due to phononic absorptions. Below these wavenumbers, these optical windows were not suited for OPTIR spectroscopy. BaF_2 could be interesting for measurements at lower wavenumbers compared to CaF_2. However, BaF_2 is highly fragile and will not be further considered.

The Raman spectrum of the CaF_2 window (Figure 4) is quite complex, with many vibrational modes in the range of 50–750 cm^{-1}. The Raman spectrum of highly pure calcium fluoride consists of a single mode at 321 cm^{-1} [19]. More complex Raman spectra were reported for CaF_2-containing impurities, such as Er [19]. For pure ZnS, the Raman spectrum should display an intense mode at 348 cm^{-1} and some weaker vibrational modes [20]. The measured Raman spectra of both compounds displayed several modes, suggesting that the optical windows contain impurities. However, as we will see in the following, this is not a problem for their use as optical windows for Raman or OPTIR spectroscopy, as the focalization of the laser beam occurs a few millimeters outside the optical windows.

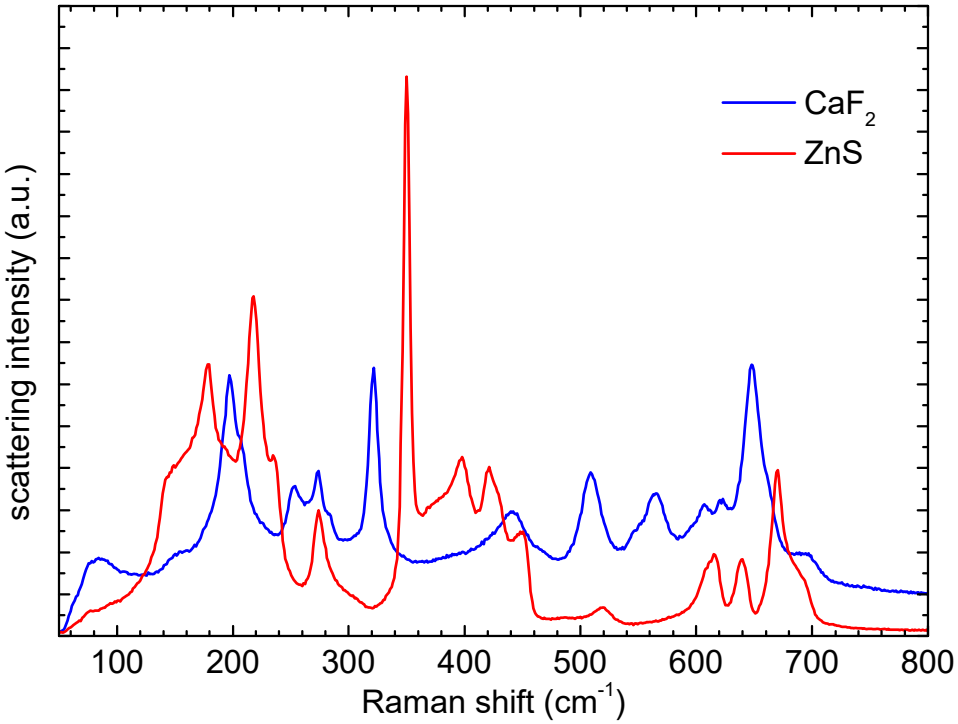

Figure 4. Raman spectra of the CaF_2 and ZnS optical windows used for this study.

3.3. Optical Photothermal Infrared Spectroscopy Measurements

Figure 5 displays a comparison of the optical images of compacted $FeCO_3$ powders used to evaluate the performances of the cell equipped with a ZnS window for OPTIR using the 10× optical objective. When the optical window is in place, one can see the presence of the powder grains (Figure 5b). The quality of the image is only slightly lower than that of the same sample measured without the optical window (Figure 5a). The presence of grains can be better appreciated at high magnification (50×, Figure 5c). Figure 5d reports the comparison between the spectra measured without any optical window and with the CaF_2 and ZnS windows in place. $FeCO_3$ displays a clear, broad absorption band between 1200 and 1600 cm^{-1}. In the previous literature, the peak observed at 1364 cm^{-1} was assigned to the CO_3 asymmetric stretching mode, $\nu_{as}(CO_3)$ [21]. It is interesting to note the absence of the O-H bending, δ(O–H), usually found around 1654 cm^{-1} in hydrated samples. The spectra measured with the sample covered by the optical windows appear slightly less defined; however, the same band is present.

In Figure S1 of the Supporting information, we compare the spectra of a Whatman separator with and without the optical window in place. In both cases, absorbance peaks are observed.

One can note that using a cheap (EUR 7) CaF_2 optical window, good-quality images and spectra can be obtained. Slightly better images can be obtained with thinner but more expensive (EUR 35 each) ZnS optical windows.

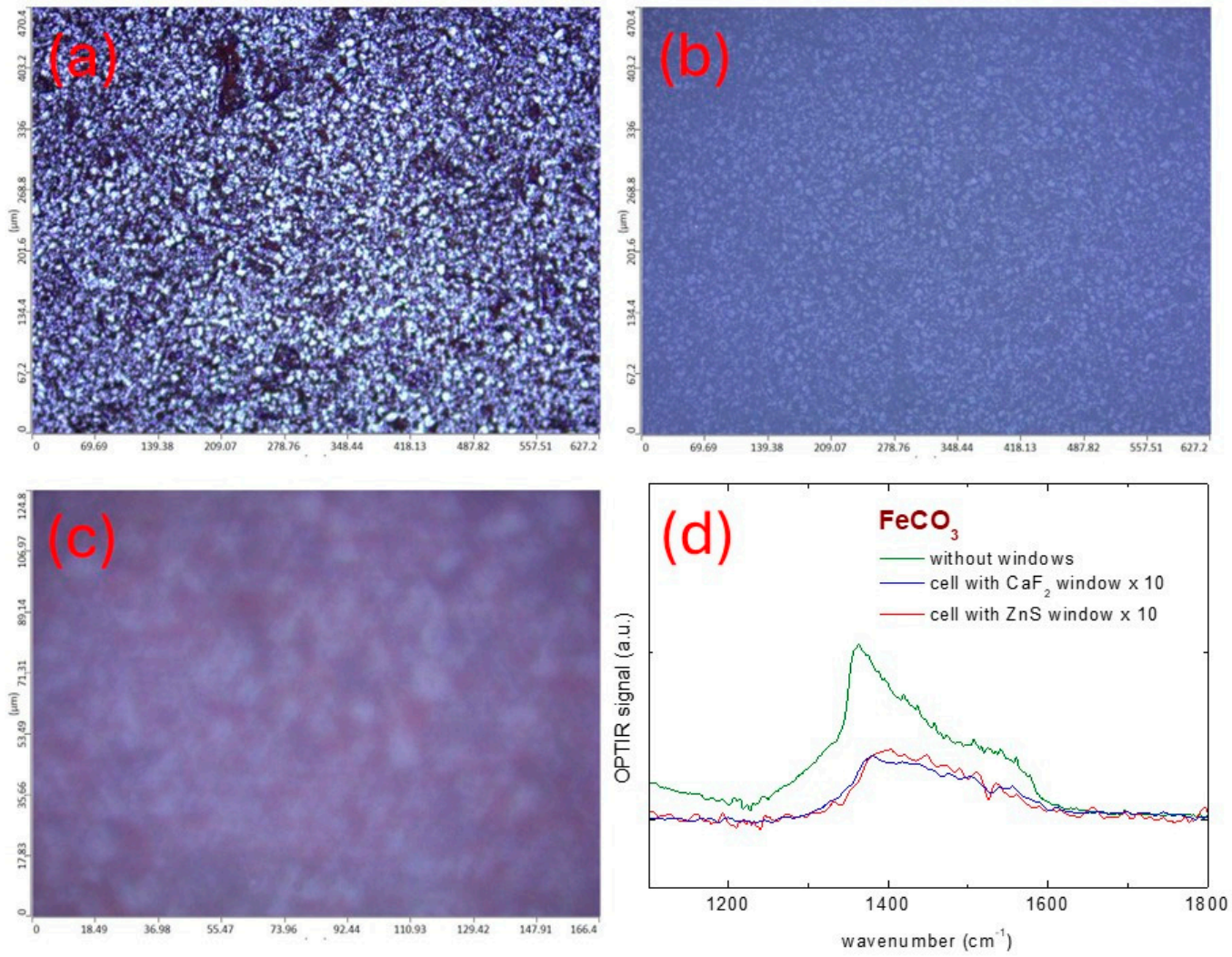

Figure 5. Optical images of the $FeCO_3$ powders measured by a 10x objective of the OPTIR instrument outside (**a**) and inside (**b**) the cell equipped with a ZnS window. The same sample is visualized by the 50× optical objective used for IR measurements (**c**). The X and Y scales on panels (**a**–**c**) are in µm. The comparison of the OPTIR spectra collected outside and inside the two cells is reported in panel (**d**).

3.4. Raman Spectroscopy Measurements

Crystalline silicon is one of the standards for the calibration of Raman spectrometers. Figure 6 reports the optical images recorded on a piece of a Si wafer measured with and without the ZnS/CaF_2 windows in place. Even when recording the images through the optical window, small imperfections of the sample surface can be appreciated, witnessing the feasibility of imaging during Raman measurements. The Raman spectra measured with and without the CaF_2 and ZnS window acquired with the same acquisition times are reported in Figure 6c. As expected, the scattering intensity measured through the optical windows was reduced precisely by a factor of 2 in the case of ZnS and a factor of 7 for the CaF_2 window; however, the spectral shape and features were nicely preserved. The peak at 520 cm^{-1}, assigned to the transversal optical (TO) phonon of crystalline Si [22], was clearly visible. The weak band centered around 290 cm^{-1} can be assigned to the overtone of the transversal acoustic phonon mode [23], while the overtone of the transversal optic phonon is centered around 925 cm^{-1} [24].

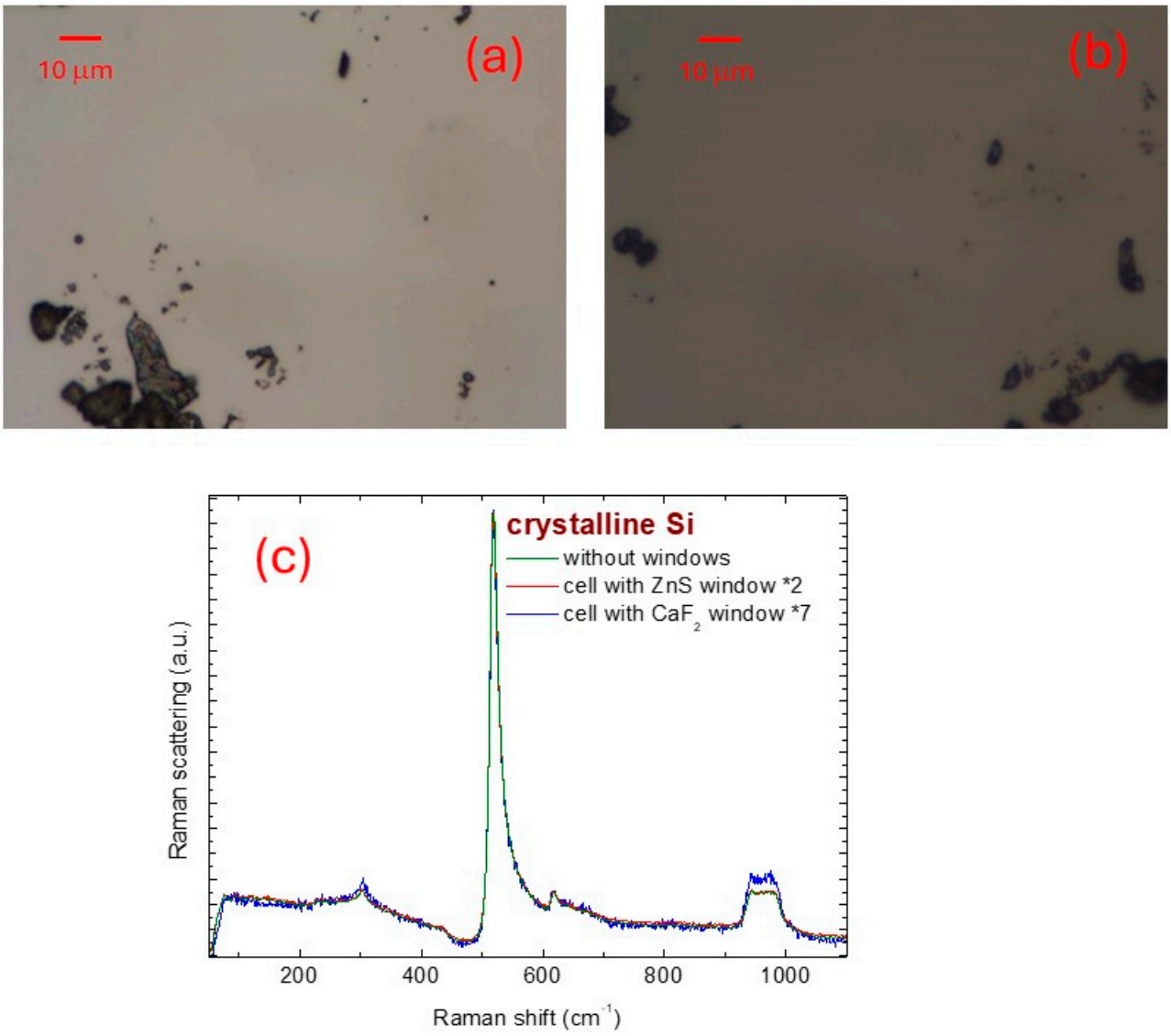

Figure 6. Optical images of a crystalline Si sample acquired in the Raman spectrometer outside (**a**) and inside (**b**) the cell with a CaF_2 optical window. The comparison of the spectra measured outside and inside the cells is reported in panel (**c**).

Notice that the presence of defects and impurities in the optical windows, as witnessed by the highly structured Raman spectra reported in Figure 4, does not modify the Raman spectrum of Si. This is due to the fact that the optical system is confocal, thus collecting only the photons emitted by a limited depth of field above and below the focal plane of the laser beam.

In Figure S2 of the Supporting information, we compare the Raman spectrum of $LiCoPO_4$ measured with or without the CaF_2 optical window.

Similarly to the case of OPTIR experiments, good quality Raman measurements can be obtained even using a cheap (EUR 7) CaF_2 optical window.

3.5. Far-Infrared Reflectance Measurements

The last application of the 3D printed cell was for far-infrared reflectance measurements. In this case, optical images were not acquired as the optics of the microscope are optimized for infrared light. Figure 7 reports the comparison of the reflectance spectrum of Li_2CO_3 powders, pressed in a pellet, in the wavenumber range between 120 and 650 cm^{-1}, with the sample placed outside and inside the cell equipped with a diamond win-

dow. The curves nicely overlap. To the best of our knowledge, no far-infrared reflectance spectrum of Li_2CO_3 has been previously reported. However, there are some studies of the transmittance above 600 cm^{-1} [25] and absorbance in Nujol between 300 and 600 cm^{-1} [26] and below 300 cm^{-1} [27]. The literature about Li_2CO_3 indicates that the vibrational bands above 600 cm^{-1} correspond to the internal modes of the CO_3^{2-} ions [25,26]. Six modes centered between 300 and 600 cm^{-1} are expected to correspond to the asymmetric LiO_4 stretching modes or the Li translational lattice modes [26]; however, only four of them were experimentally observed due to possible degeneracy. They were found to be centered at 402, 459, 517, and 549 cm^{-1} in $^6Li_2CO_3$ and 375, 433, 486, and 513 cm^{-1} in $^7Li_2CO_3$ [26]. Below 300 cm^{-1}, three bands, including one shoulder, were reported, with the frequency of the maxima at 254, 140, and 133 cm^{-1} [26]. In this region, practically, there is no isotope effect, as the bands are attributable to the CO_3^{2-} translational or rotational lattice vibrations [26].

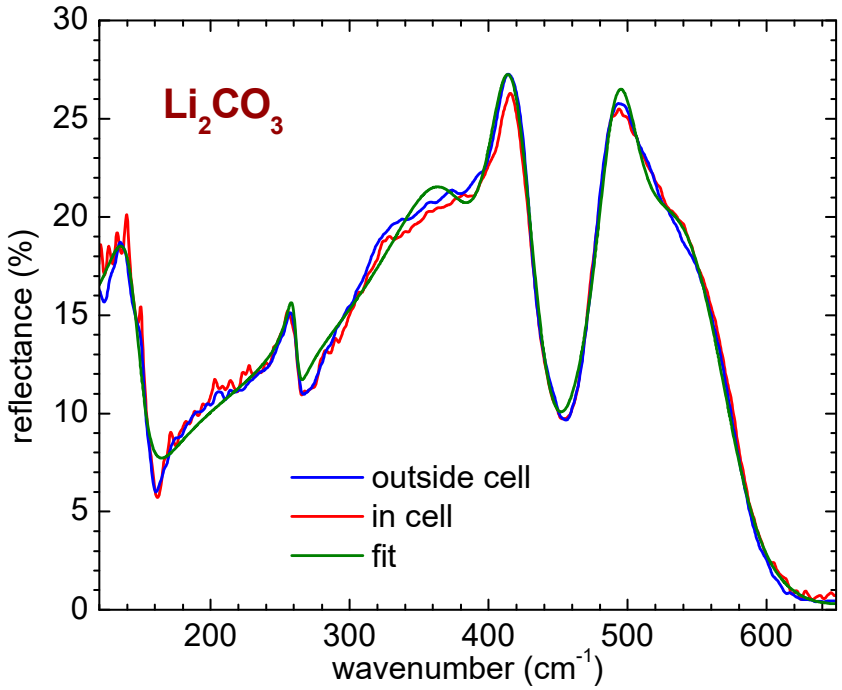

Figure 7. Comparison of the far-infrared reflectance spectrum of Li_2CO_3 measured outside and inside a cell equipped with a diamond window. The green line is the best fit obtained using the Drude-Lorentz model.

The reflectance spectrum of Li_2CO_3 measured outside the cell was fitted utilizing the RefFIT software [28], considering the lowest number of modes that allowed obtaining a reasonable description of the experimental spectrum through the Drude–Lorentz model. The best-fit line is reported in Figure 7, compared to the experimental data. A reasonable fit can be obtained with six Lorentz peaks centered around 141, 260, 366, 409, 486, and 524 cm^{-1}. The best-fit parameters, including the transverse frequency, plasma frequency, and scattering rate of the six peaks, are reported in Table 1.

The peak maxima are close to those reported [26] for Li_2CO_3 containing only the ^7Li isotope. This can be easily understood, as the natural abundance of this isotope is 92.5%.

A last remark concerns the high cost (EUR 480) of the diamond optical window utilized for the far-infrared measurements. As a future direction, the use of much cheaper plastic windows should be explored.

Table 1. Best fit parameters for the reflectance spectrum of Li_2CO_3 (transverse frequency ω_0, plasma frequency ω_p, and scattering rate γ).

Transverse Frequency (cm^{-1})	Plasma Frequency (cm^{-1})	Scattering Rate (cm^{-1})
141.2	109.6	28.1
260.3	52.1	8.2
365.9	319.7	76.6
409.4	222.4	34.4
486.1	221.4	31.5
523.5	230.3	80.0

4. Conclusions

In conclusion, a 3D printed cell was developed that can be adapted for various spectroscopic techniques working in a quasi-normal reflectance geometry, preserving samples from contamination by atmospheric moisture and gases. Both a very cheap and thicker CaF_2 and a more expensive and thinner ZnS optical window allowed the acquisition of OPTIR and Raman spectra; the level of impurities present in these windows did not influence the acquisitions. Optical imaging of samples could also be obtained for both kinds of windows. To extend the use of the cell to far-infrared reflectance measurements, the cell was adapted to accommodate a thin artificial diamond window, which allowed measuring a high-quality spectrum of Li_2CO_3. As a future development, the use of plastics, such as polyethylene, for the far-infrared range will be explored to significantly decrease the cost of these measurements.

Supplementary Materials: The following supporting information can be downloaded at https://www.mdpi.com/article/10.3390/instruments8040054/s1, Figure S1. Comparison of the OPTIR spectrum of a Whatman separator measured with and without the CaF_2 window in place. On the right, the optical image of the separator through the optical window is reported. One can see the fibers that compose the sample in Figure S2. Comparison of the Raman spectrum of $LiCoPO_4$ powders measured with and without the CaF_2 window in place.

Author Contributions: Conceptualization, A.P.; methodology, A.P.; software, A.P.; investigation, A.P., A.C., M.D.P., F.C. and F.B.; resources, A.P., S.B., F.C. and F.B.; data curation, A.P.; writing—review and editing, A.P.; funding acquisition, A.P. and S.B. All authors have read and agreed to the published version of the manuscript.

Funding: The authors acknowledge financial support from "ORgANics for Green Electrochemical Energy Storage Project (ORANGEES)" funded by MASE "PT 2019–2021, DD 27.10.2021 bando a, DD 05.08.2022". SB would also like to acknowledge Sapienza through the RM123188F6EF1968 and RM122181677EDA1D actions. The contribution of AC to this study was carried out within the NEST—Network for Energy Sustainable Transition and received funding from the European Union Next-Generation EU (PIANO NAZIONALE DI RIPRESA E RESILIENZA (PNRR)—MISSIONE 4 COMPONENTE 2, INVESTIMENTO 1.3—D.D. 1561 11/10/2022, B53C22004070006). This manuscript reflects only the authors' views and opinions. Neither the European Union nor the European Commission can be considered responsible for them. All Sapienza staff within the NEST project participate in this action under the frame of the grant PE2421852F05911E.

Data Availability Statement: The original contributions presented in this study are included in the article/supplementary material. Further inquiries can be directed to the corresponding author(s). Moreover, the stl files of cells developed for optical windows of diameter 12 mm and thickness 1 mm or diameter 12.7 mm and thickness 0.5 mm were deposited in the Zenodo repository (DOI: 10.5281/zenodo.13985862).

Acknowledgments: We acknowledge Synchrotron SOLEIL for the provision of synchrotron radiation facilities during beamtime 20231278. We would also like to thank Stéphanie Blanchandin, manager of the Chemistry Laboratories of Soleil, for the use of the LabRAM Soleil Raman Microscope by Horiba Scientific and her help with the instrument.

Conflicts of Interest: The authors declare no conflicts of interest.

References

1. Letcher, T.M. (Ed.) *Storing Energy with Special Reference to Renewable Energy Sources*, 2nd ed.; Elsevier: Amsterdam, The Netherlands, 2022.
2. Maddukuri, S.; Malka, D.; Chae, M.S.; Elias, Y.; Luski, S.; Aurbach, D. On the challenge of large energy storage by electrochemical devices. *Electrochim. Acta* **2020**, *354*, 136771. [CrossRef]
3. Nasajpour-Esfahani, N.; Garmestani, H.; Bagheritabar, M.; Jasim, D.J.; Shohreh Dadkhah, T.; Firoozeh, H. Comprehensive review of lithium-ion battery materials and development challenges. *Renew. Sustain. Energy Rev.* **2024**, *203*, 114783. [CrossRef]
4. Sarra, A.; Brutti, S.; Palumbo, O.; Capitani, F.; Borondics, F.; Appetecchi, G.B.; Carboni, N.; AbdulAhad, S.; Geaney, H.; Ryan, K.; et al. Solid–Electrolyte Interface Formation on Si Nanowires in Li-Ion Batteries: The Impact of Electrolyte Additives. *Batteries* **2023**, *9*, 148. [CrossRef]
5. Rodrigues de Souza Leão, A.; Pires Batista, A.C.; Barbosa Alves, P.; Silveira de Castro, Z. Polymeric composites in extrusion-based additive manufacturing: A systematic review. *Polym. Compos.* **2024**, *45*, 6741–6770. [CrossRef]
6. Heidt, B.; Rogosic, R.; Leoné, N.; Brás, E.J.S.; Cleij, T.J.; Harings, J.A.W.; Diliën, H.; Eersels, K.; van Grinsven, B. Topographical Vacuum Sealing of 3D-Printed Multiplanar Microfluidic Structures. *Biosensors* **2021**, *11*, 395. [CrossRef] [PubMed]
7. Hudson, A.D.; Jamieson, O.; Crapnell, R.D.; Rurack, K.; Soares, T.C.C.; Mecozzi, F.; Laude, A.; Gruber, J.; Novakovica, K.; Peeters, M. Dual detection of nafcillin using a molecularly imprinted polymer-based platform coupled to thermal and fluorescence read-out. *Mater. Adv.* **2021**, *2*, 5105–5115. [CrossRef]
8. Mahmood, R.I.; Mahmoud, K.I.; Ghazi, A. A low cost microscope prototype. *AIP Conf. Proc.* **2021**, *2372*, 030004.
9. Botero-Valencia, J.; Reyes-Vera, E.; Ospina-Rojas, E.; Prieto-Ortiz, F. A Portable Tool for Spectral Analysis of Plant Leaves That Incorporates a Multichannel Detector to Enable Faster Data Capture. *Instruments* **2024**, *8*, 24. [CrossRef]
10. Schimo, G.; Hassel, A.W. 3D printed double flow cell for local through-thickness anodization in aluminium. *Electrochem. Commun.* **2016**, *69*, 84–88. [CrossRef]
11. Maierhofer, M.; Maier, M.C.; Gruber-Woelfler, H.; Mayr, T. Inline monitoring of high ammonia concentrations in methanol with a customized 3D printed flow cell. *J. Flow Chem.* **2021**, *11*, 717–723. [CrossRef]
12. Sakata, K.; Bilal, M.; Sakairi, M.; Murata, T. Local Electrochemical Measurements by 3D Printed Sf-MDC Equipped with Optical Microscope. *J. Electrochem. Soc.* **2021**, *168*, 061505. [CrossRef]
13. Grazioli, C.; Lanza, E.; Abate, M.; Bontempelli, G.; Dossi, N. Lab-on kit: A 3D printed portable device for optical and electrochemical dual-mode detection. *Talanta* **2024**, *275*, 126185. [CrossRef] [PubMed]
14. Katseli, V.; Thomaidis, N.; Economou, A.; Kokkinos, C. Miniature 3D-printed integrated electrochemical cell for trace voltametric Hg(II) determination. *Sens. Actuators B Chem.* **2020**, *308*, 127715. [CrossRef]
15. Dossi, N.; Toniolo, R.; Terzi, F.; Grazioli, C.; Svigelj, R.; Gobbi, F.; Bontempelli, G. A Simple Strategy for Easily Assembling 3D Printed Miniaturized Cells Suitable for Simultaneous Electrochemical and Spectrophotometric Analyses. *Electroanalysis* **2020**, *32*, 291–300. [CrossRef]
16. dos Santos, M.F.; Katic, V.; dos Santos, P.L.; Pires, B.M.; Formiga, A.L.B.; Bonacin, J.A. 3D-Printed Low-Cost Spectroelectrochemical Cell for In Situ Raman Measurements. *Anal. Chem.* **2019**, *91*, 10386–10389. [CrossRef] [PubMed]
17. OpenSCAD. The Programmers Solid 3D CAD Modeller. Available online: https://openscad.org/index.html (accessed on 23 October 2024).
18. Dolmatov, V.Y.; Kulakova, I.I.; Myllymäki, V.; Vehan, A.; Bochechka, A.A.; Panova, A.N.; Nguyen, B.T.T. IR spectra of diamonds of different origins and upon different purification procedures. *J. Superhard Mater.* **2016**, *38*, 58–65. [CrossRef]
19. Gee, A.R.; O'Shea, D.C.; Cummins, H.Z. Raman scattering and fluorescence in calcium fluoride. *Solid State Commun.* **1966**, *4*, 43–46. [CrossRef]
20. Fairbrother, A.; Izquierdo-Roca, V.; Fontané, X.; Ibáñez, M.; Cabot, A.; Saucedo, E.; Pérez-Rodríguez, A. ZnS grain size effects on near-resonant Raman scattering: Optical non-destructive grain size estimation. *CrystEngComm* **2014**, *16*, 4120–4125. [CrossRef]
21. Saaid, F.I.; Arsyad, A.; Azman, N.S.H.; Kumar, A.; Yang, C.-C.; Tseng, T.-Y.; Winie, T. The synergistic effect of iron cobaltite compare to its single oxides as cathode in supercapacitor. *J. Electroceramics* **2020**, *44*, 183–194. [CrossRef]
22. Parker, J.H., Jr.; Feldman, D.W.; Ashkin, M. Raman Scattering by Silicon and Germanium. *Phys. Rev.* **1967**, *155*, 712–714. [CrossRef]
23. Smit, C.; van Swaaij, R.A.C.M.M.; Donker, H.; Petit, A.M.H.N.; Kessels, W.M.M.; van de Sanden, M.C.M. Determining the Material Structure of Microcrystalline Silicon from Raman Spectra. *J. Appl. Phys.* **2003**, *94*, 3582–3588. [CrossRef]
24. Wang, R.; Zhou, G.; Liu, Y.; Pan, S.; Zhang, H.; Yu, D.; Zhang, Z. Raman Spectral Study of Silicon Nanowires: High-Order Scattering and Phonon Confinement Effects. *Phys. Rev. B* **2000**, *61*, 16827. [CrossRef]
25. Buijs, K.; Schutte, C.J.H. The infra-red spectra and structures of Li_2CO_3 and anhydrous Na_3CO_3. *Spectrochim. Acta* **1961**, *17*, 927–932. [CrossRef]
26. Hase, Y.; Yoshida, I.V.P. Li-O Raman bands of $^6Li_2CO_3$ and $^7Li_2CO_3$. *Spectrochim. Acta A* **1979**, *35*, 377–378.
27. Hase, Y.; Yoshida, I.V.P. Low frequency bands of Li_2CO_3 crystal. *Spectrochim. Acta A* **1979**, *35*, 379–382. [CrossRef]
28. Kuzmenko, A.B. Kramers-Kronig constrained variational analysis of optical data. *Rev. Sci. Instr.* **2005**, *76*, 083108. [CrossRef]